Open access • Journal Article • DOI:10.1038/NCHEMBIO.1437

Ubiquinone accumulation improves osmotic-stress tolerance in Escherichia coli

Daniel C. Sévin, Uwe Sauer

Institutions: École Polytechnique Fédérale de Lausanne

Published on: 01 Apr 2014 - Nature Chemical Biology (Nature Publishing Group)

Topics: Osmotic shock and Osmoprotectant

Ubiquinone accumulation improves osmotic-stress tolerance in Escherichia coli

Sévin, Daniel C ; Sauer, Uwe

Abstract: Bacteria are thought to cope with fluctuating environmental solute concentrations primarily by adjusting the osmolality of their cytoplasm. To obtain insights into underlying metabolic adaptions, we analyzed the global metabolic response of Escherichia coli to sustained hyperosmotic stress using non-targeted mass spectrometry. We observed that 52% of 1,071 detected metabolites, including known osmoprotectants, changed abundance with increasing salt challenge. Unexpectedly, unsupervised data analysis revealed a substantial increase of most intermediates in the ubiquinone-8 (Q8) biosynthesis pathway and a 110-fold accumulation of Q8 itself, as confirmed by quantitative lipidomics. We then demonstrate that Q8 is necessary for acute and sustained osmotic stress tolerance using Q8 mutants and tolerance rescue through feeding non-respiratory Q8 analogues. Finally, in vitro experiments with artificial liposomes reveal mechanical membrane stabilization as a principal mechanism of Q8-mediated osmoprotection. Thus, we find that besides regulating intracellular osmolality, E. coli enhances its cytoplasmic membrane stability to withstand osmotic stress.

DOI: https://doi.org/10.1038/NCHEMBIO.1437

Originally published at:
Sévin, Daniel C; Sauer, Uwe (2014). Ubiquinone accumulation improves osmotic-stress tolerance in Escherichia coli. Nature Chemical Biology, 10(4):266-272.
DOI: https://doi.org/10.1038/NCHEMBIO.1437

Ubiquinone Accumulation Improves Osmotic Stress Tolerance in *Escherichia coli*

Revised manuscript (2nd and final revision)

Authors: Daniel C. Sévin[1,2] and Uwe Sauer[1]*

Affiliations: [1]Institute of Molecular Systems Biology, ETH Zurich, 8093 Zurich, Switzerland

[2]PhD Program on Systems Biology, Life Science Zurich, 8057 Zurich, Switzerland

*To whom correspondence should be addressed: sauer@ethz.ch

Key words: Osmotic stress tolerance, membrane, membrane stability, metabolomics, stress response

Abstract

Bacteria are thought to cope with fluctuating environmental solute concentrations primarily by adjusting the osmolality of their cytoplasm. To obtain insights into underlying metabolic adaptions, we analyzed the global metabolic response of *Escherichia coli* to sustained hyperosmotic stress using non-targeted mass spectrometry. We observed that 52% of 1,071 detected metabolites, including known osmoprotectants, changed abundance with increasing salt challenge. Unexpectedly, unsupervised data analysis revealed a substantial increase of most intermediates in the ubiquinone-8 (Q8) biosynthesis pathway and a 110-fold accumulation of Q8 itself, as confirmed by quantitative lipidomics. We then demonstrate that Q8 is necessary for acute and sustained osmotic stress tolerance using Q8 mutants and tolerance rescue through feeding non-respiratory Q8 analogues. Finally, *in vitro* experiments with artificial liposomes reveal mechanical membrane stabilization as a principal mechanism of Q8-mediated osmoprotection. Thus, we find that besides regulating intracellular osmolality, *E. coli* enhances its cytoplasmic membrane stability to withstand osmotic stress.

Introduction

Bacteria are frequently exposed to abruptly changing solute concentrations in their environments. Desiccation in biofilms, tidal sweeps of salt water into rivers or sudden nutrient bursts in the gut of host organisms increase the extra-cellular osmolality, whereas rainfall or retreating tides decrease osmolality. Since the cytoplasmic membrane is impermeable to most large and polar solutes, trans-membrane concentration gradients of non-permeating compounds are established that are compensated for by freely diffusing water molecules. The consequences are changing cellular volume and turgor pressure that exert strong mechanical forces on the cytoplasmic membrane and associated proteins and, if too high, preclude growth of the bacterium and eventually cause cell death[1]. To cope with osmotic stress, bacteria evolved several strategies such as adapting their intracellular osmolality[2–4] or increasing their cell wall stability[5], allowing them to grow in a broad range of solute concentrations.

The regulation of intracellular osmolality by transport or biosynthesis of compatible solutes is believed to be the principal osmoprotection response in the gram-negative bacterium *Escherichia coli*[6] that can be mediated by several molecular mechanisms. First, *E. coli* controls in- and outflux of water and other small molecules by activation of aquaporins as an immediate response to sudden changes in osmotic pressure[7]. Second, it regulates intracellular potassium levels by adjusting the expression of potassium transporters such as Kup, KdpFABC or TrkA for transient adaptation to short-term osmotic stress[8]. Third, in case of prolonged osmotic stress, *E. coli* can take up the osmoprotectants glycine betaine and proline from the environment via the *proVWX*-encoded ABC transporter or synthesize glycine betaine from the extracellular precursor choline[2,9,10]. Fourth, if no extracellular compatible solutes are available, *E. coli* induces expression of trehalose-6-phosphate synthase (OtsA) and phosphatase (OtsB) to produce high intracellular concentrations of the non-reducing disaccharide trehalose from the precursors UDP-glucose and glucose 6-phosphate, conveying long-term resistance to sustained osmotic stress[11–13]. Quantitative studies indicated,

however, that the amounts of compatible solutes produced by *E. coli* may not be sufficient to maintain cell turgor exclusively based on increasing intracellular osmolality, implying accompanying effects such as molecular crowding[14]. Besides adjusting intracellular osmolality, other bacteria have been shown to modify their cell wall structure upon osmotic stress[5], but this mechanism has not been observed in *E. coli*. Virtually all known osmoprotection mechanisms in *E. coli* therefore relate to the modulation of intracellular osmolality. The only exception are molecular dynamics studies that demonstrated an interaction between accumulated trehalose with membrane lipid head groups[15], although this effect was found to be quantitatively insufficient to fully account for the resistance of membranes to strong osmotic stress[16].

Since nearly all known osmoprotection mechanisms are related to metabolism, we aimed to obtain global and unbiased insights into the metabolic adaptation of *E. coli* to sustained osmotic stress. Specifically, we analyzed the intracellular steady state metabolome of exponentially growing *E. coli* at six levels of sodium chloride (NaCl)-induced hyperosmotic stress. To this end, we used our previously developed non-targeted flow injection time-of-flight mass spectrometry (MS) platform[17] that allows to measure the semiquantitative levels of hundreds of intracellular metabolites. The acquired data not only shed light on complex metabolic rearrangements, but also led to the discovery of a novel mechanism for coping with osmotic stress, namely the active improvement of cell membrane stability by accumulation of the electron carrier and lipid ubiquinone-8.

Results

Osmotic stress causes complex changes in metabolism

To quantify its sensitivity to salt, *E. coli* BW25113 was cultivated at 37° C in mineral medium containing glucose as the sole carbon source, supplemented with 50 to 750 mM NaCl. The maximum specific growth rate was calculated for each NaCl concentration, yielding a half-maximal inhibitory concentration (IC_{50}) of 450 mM (**Fig. 1a**). Based on these results, we selected 6 NaCl concentrations between 50 and 500 mM that allowed for distinct exponential growth phases and sufficient biomass concentrations to permit metabolomics experiments. For each NaCl concentration we then extracted intracellular metabolites with hot water from exponentially growing *E. coli* cultures at an optical density at 600 nm of 1.0 (**Fig. 1b**). Using non-targeted flow injection time-of-flight MS[17], we detected 8,961 ions of which 535 could be annotated based on accurate mass, corresponding to up to 1,071 unique metabolites. For further analyses we considered only the 535 annotated ions and normalized all ion intensities to the values determined in cells not suffering from hyperosmotic stress, that is, grown in the presence of 50 mM NaCl. In total, 52% of the annotated ions changed abundance more than 2-fold between 50 mM NaCl and 500 mM NaCl (**Supplementary Results, Supplementary Dataset 1**), underlining the complexity and global dimension of the metabolic response to hyperosmotic stress. As expected, we found 40-fold increased intracellular concentrations of trehalose, the major osmoprotectant metabolite in *E. coli* (**Fig. 1c**). Glycine betaine and glutamate levels did not increase (**Fig. 1c**), confirming that these compounds are only used as osmoprotectants if available in the environment[10]. Moreover, we observed an over 10-fold decrease of various cyclic nucleotide monophosphate levels with increasing salt concentration (**Fig. 1c**), supporting the hypothesis that cAMP-based modulation of CRP activity triggers the *E. coli* response to osmotic stress[18,19].

To obtain an overview of the global metabolic response to osmotic stress, we performed unsupervised *k*-means clustering of all metabolite ion fold-changes over increasing salt concentration, specifying a number of 4 clusters (**Fig. 2a**). Cluster 1 contains 98 ions that decrease

with increasing salt levels. Cluster 2 contains 348 non-responsive ions without a clear trend. Cluster 3 contains 24 ions that increase more than 100-fold with increasing salt levels. Cluster 4 contains 65 moderately increasing (~30-fold) ions. Metabolic pathway enrichment analysis was performed to identify metabolically connected groups of compounds that correlated with salt levels in clusters 1, 3 and 4 (**Fig. 2b**). The decreasing metabolites in cluster 1 were significantly enriched for nucleotide and amino acid biosynthesis, probably reflecting a lower demand for these biosynthetic precursors as an indirect consequence of the reduced growth rates at elevated salt levels. The moderately increasing metabolites in cluster 4 were mainly found in pathways for uptake and biosynthesis of carbohydrates such as starch, sucrose or galactose, consistent with the osmoprotective properties of sugars and other poly-hydroxylated compounds[20]. The strongly increasing metabolites in cluster 3 were significantly enriched in only four pathways, namely the phosphotransferase system, starch and sucrose metabolism, galactose metabolism, and ubiquinone/terpenoid quinone biosynthesis. Whereas the accumulation of carbohydrates was anticipated, the major increase in the concentrations of compounds participating in ubiquinone biosynthesis was entirely unexpected, and was not coupled to increased gene expression as shown by green fluorescence reporter assays with the ubiquinone biosynthesis genes *ubiC*, *ubiE*, *ubiF*, *ubiG* and *ubiX* (**Supplementary Fig. 1**) in agreement with previous gene expression data[21]. Essentially all intermediates in the ubiquinone biosynthetic pathway accumulated on average 40-fold, consistent with a high demand caused by the 250-fold accumulation of the pathway end-product ubiquinone-8 (Q8) at high salt concentrations (**Fig. 3a**).

Because the aqueous extraction procedure used in our metabolomics experiment was not optimal to capture lipids such as Q8, we extracted *E. coli* cells grown in isosmotic and hyperosmotic conditions with chloroform and methanol[22] and measured lipid levels by flow injection MS[17]. In agreement with our previous metabolomics experiment, non-targeted lipidomics confirmed a 110-fold salt-dependent increase in Q8 levels, the highest fold-change among all detected lipids, concomitant with an apparent decrease of shorter-chain isoprenoid lipids (**Fig. 3b**). We subsequently

quantified Q8 levels relative to the main *E. coli* membrane phospholipids diacyl-phosphatidylethanolamine and diacyl-phosphatidylglycerol by MS using dilution series of commercial lipid standards as reference. Whereas under isosmotic conditions Q8 was below the quantification limit, its fraction increased to 1% (w/w) upon osmotic stress (**Fig. 3c**), implying that Q8 contributes substantially to the membrane lipid composition. Since to our knowledge Q8 accumulation in response to hyperosmotic stress has never been described, we investigated in the following whether it serves a functional role in osmotic stress tolerance.

Q8 is necessary for osmotic stress tolerance *in vivo*

Since Q8 can act as a radical scavenger[23], we first wanted to exclude that its accumulation was due to oxidative stress, which has been postulated to be an indirect consequence of osmotic stress[24,25]. We therefore measured the levels of reactive oxygen species (ROS) at low and high salt concentrations in wild-type *E. coli* and a Δ*ubiG* deletion mutant that is unable to synthesize Q8[26]. ROS levels were only marginally elevated under hyperosmotic conditions and were generally reduced in the Δ*ubiG* mutant (**Supplementary Fig. 4a**). Moreover, the ratio of the radical scavenger glutathione to its oxidized form did not decrease at higher salt levels (**Supplementary Fig. 4b**) and cells did not secrete oxidized glutathione to detectable levels, as one would expect if intracellular ROS increased with osmotic stress[27]. These results demonstrate that cells in our experiments did not suffer severely from oxidative stress, which is further corroborated by the accumulation of not only oxidized Q8 but also its reduced $Q8H_2$ form (**Fig. 3a**).

To confirm that the observed ubiquinone accumulation indeed contributes to resistance against sustained hyperosmotic stress and is not merely a side effect of a global stress response, we tested the salt sensitivity of the Δ*ubiG* deletion mutant. Indeed, the IC_{50} value of the Δ*ubiG* mutant for NaCl was drastically reduced compared to wild-type (**Fig. 4a** and **b**). Moreover, the decrease of the Δ*ubiG* mutant's salt tolerance was significantly more severe than in the Δ*galU*, Δ*otsA* and Δ*otsB* mutants that are unable to synthesize the major osmoprotectant trehalose[12] (**Fig. 4b**). Thus, the presence of Q8 is necessary for resistance to osmotic stress. To exclude that the osmoprotective

effect is more trivially related to the known role of Q8 as a membrane-localized electron carrier in the respiratory chain[28], we tested salt sensitivity of the wild-type strain and the Δ*ubiG* mutant during fermentative anaerobic growth where respiration is inactive. Since the anaerobic salt tolerance of both strains was unchanged compared to the aerobic condition (**Fig. 4a** and **b**), we can exclude respiratory chain interruption as the cause for increased salt sensitivity of the Δ*ubiG* mutant. The independence of osmotolerance from respiration is further corroborated by the finding that salt tolerance of the Δ*ubiG* mutant could be restored to nearly wild-type levels by extracellular addition of the human Q8 analog ubiquinone-10 (Q10) (**Fig. 4a** and **b**). Q10 cannot substitute Q8 as an efficient electron carrier in *E. coli* as judged by low growth rate of the Q10-supplemented Δ*ubiG* mutant in isosmotic conditions (**Fig. 4a** and **b**). Collectively, these experiments demonstrate that Q8 is necessary for osmotic stress tolerance in *E. coli* and that this tolerance improvement cannot be explained by the so far known functions of Q8 as a radical scavenger or respiratory electron carrier.

We hypothesized that Q8-mediated osmoprotection is caused by mechanical stabilization of the cytoplasmic membrane because Q10 with similar physicochemical properties can restore osmotolerance in a Δ*ubiG* mutant. The cytoplasmic membrane is involved in maintaining size and shape of bacterial cells and *E. coli* is known to passively decrease in volume upon hyperosmotic stress[29]. To elucidate whether the presence of ubiquinone affects cellular morphology upon an osmotic shock, we subjected wild-type *E. coli* as well as the Δ*ubiG* mutant and the Δ*ubiG* mutant supplemented with Q10 to different intensities of acute osmotic shock and analyzed cell morphology by microscopy within 5 minutes. Indeed, Δ*ubiG* cells were significantly smaller than wild-type and supplementation with Q10 increased the cell volume of the Δ*ubiG* mutant back to wild-type levels (**Fig. 4c** and **d**), indicating that the physical presence of Q8 in the membrane helps to prevent a strong volume decrease upon osmotic shock. From molecular dynamics simulations it is known that the ability of vesicles to resist mechanical forces decreases with increasing membrane surface area[30], implying that larger cells require more stable cell envelopes to resist osmotic pressure. Thus, the

small-size morphotype of Δ*ubiG* mutants lacking the possibility to accumulate Q8 supports our hypothesis that Q8 is involved in mechanical membrane stabilization upon osmotic shock.

Which moiety of the Q8 molecule is responsible for its osmoprotective properties? Q8 consists of a decorated benzoquinone ring with an attached hydrophobic chain of eight isoprenyl subunits (**Fig. 4e**). To test whether the length of the polyprenyl chain influences the osmoprotective effect of ubiquinone, we cultivated the Δ*ubiG* mutant in the presence of different ubiquinones with zero (Q0), two (Q2), four (Q4) or ten (Q10) isoprenyl subunits and microscopically analyzed its morphology after a strong osmotic shock. A positive correlation was observed between post-shock cell size and polyprenyl chain length, but only Q10 restored wild-type cell size of the Δ*ubiG* mutant (**Fig. 4f**). Chain length-dependent morphotype restoration was also observed with different non-quinone isoprenoids carrying a polar hydroxyl headgroup but was not successful with lycopene that lacks a polar headgroup (**Supplementary Fig. 5**). This implies that a polar headgroup is necessary for osmoprotection by isoprenoids *in vivo* but that the chemical nature of this headgroup is of secondary importance. We conclude that osmoprotection by ubiquinones is conveyed by the octaprenyl chain and not by the benzoquinone moiety, and that chains of sufficient length are required for wild-type osmotolerance. This finding is consistent with previous *in vitro* data showing that the polyprenyl chain length of ubiquinones influences melting profile and surface pressure of artificial phospholipid membranes[31,32]. Further circumstantial evidence for our conclusion that Q8 mechanically stabilizes the cytoplasmic membrane of *E. coli* comes from the fact that membranes of halotolerant and halophilic archaea are almost exclusively composed of lipids with saturated isopranyl side chains[33], which are known to be crucial for their survival in extreme saline environments[34,35].

Q8 improves stability of artificial liposomes

To directly test whether ubiquinone improves the mechanical stability of lipid membranes rather than properties of membrane-associated proteins, we prepared protein-free artificial liposomes with different Q10 contents and subjected them to acute hyperosmotic stress by increasing the osmolality of the external buffer within 1 second (**Fig. 5**). Whereas 1% (w/w) Q10 did not markedly improve

liposome stability, a concentration of 5% (w/w) Q10 allowed most liposomes to withstand a strong osmotic shock with 1M NaCl. Liposomes without Q10 started to disintegrate already at 300 mM NaCl and were almost completely destroyed at 500 mM NaCl. Liposome stability was also enhanced by the non-quinone isoprenoids solanesol and lycopene (**Supplementary Fig. 6**), confirming that it is the polyprenyl moiety of Q10 and not its benzoquinone headgroup that conveys osmoprotection. The observation that lycopene has an osmoprotective effect on liposomes but not on living cells could potentially be explained by different membrane assembly mechanisms that are enzymatically regulated *in vivo* in contrast to spontaneous formation occurring *in vitro*. Thus, these results demonstrate that the presence of Q10 is sufficient to increase the osmotic stress resistance of lipid membranes and that this effect can occur independently of membrane proteins. We therefore conclude that Q8 contributes to osmoprotection in *E. coli* by mechanically stabilizing its cytoplasmic membrane.

Discussion

In this study, we investigated the global metabolic response of *E. coli* to sustained hyperosmotic salt stress using non-targeted metabolomics, and unexpectedly found the respiratory electron carrier Q8 as the by far most accumulated metabolite. Data of deletion mutants defective in Q8 biosynthesis demonstrated the presence of Q8 to be essential for osmotic stress tolerance. The known roles of Q8 in the respiratory chain or as a radical scavenger cannot explain its beneficial effect because i) salt sensitivity under anaerobic conditions was unchanged and ii) salt tolerance can be restored by the addition of Q8 analogs that are not efficiently used for respiration in *E. coli*. This independence of Q8 osmoprotection from respiration is further supported by previously reported unchanged trans-membrane proton gradient and respiratory activity during osmotic stress[36]. Instead, we demonstrate through *in vitro* experiments with protein-free artificial liposomes and through *in vivo* morphotyping that Q8 enhances membrane stability, strongly suggesting a causal link between Q8 accumulation and osmotic stress resistance by direct stabilization of the cytoplasmic membrane. Because Q8 accumulated to up to 1% of main membrane lipids *in vivo* whereas liposome stabilization required at least 5% Q10 content, we cannot exclude that Q8 accumulation might additionally improve function or stability of membrane proteins by direct interactions with their membrane-localized domains[37] or by molecular crowding[14,38], or alter bioenergetic membrane properties by reducing sodium ion leakage[39].

Our summarized findings lead us to propose the following model of Q8-mediated osmoprotection in *E. coli* (**Supplementary Fig. 7**). Upon exposure to conditions of osmotic stress and apparently independent of transcriptional regulation, a yet unknown regulatory mechanism triggers the accumulation of Q8 to up to 1% of total membrane lipids. The Q8 molecule has been shown to reside flat in the center of the lipid bilayer[32,39], implying that the observed substantial accumulation of Q8 would increase the hydrophobic thickness of the cytoplasmic membrane. Intriguingly, such an effect has already been observed *in vitro* with the isoprenoid zeaxanthin, of which concentrations

between 1% and 10% increased the hydrophobic thickness of artificial lipid bilayer membranes[40]. Furthermore, the branched methyl groups of the octaprenyl moiety may interconnect the lipids within and between the monolayer leaflets by interacting with their phospholipid side chains, thus increasing membrane stability. Together, these mechanisms would make the cytoplasmic membrane more resistant to forces imposed by osmotic pressure[41].

Since the cytoplasmic membranes of archaea that are able to resist harsh environmental conditions consist mainly of isopranoid lipids[33], it is tempting to speculate that transient or permanent stabilization of biological membranes through isoprenoids may be an ancient and well-conserved property. Unlike Q8, archaeal membrane lipids are generally saturated, contain ether bonds and are, in some cases, bipolar[35]. Nevertheless, the overall structural and chemical similarity between Q8 and archaeal isopranoid lipids and our finding that isoprenoids with different headgroups can substitute for Q8 in restoring osmotolerance both *in vitro* and *in vivo* support our conclusion that increased concentrations of Q8 indeed stabilize membranes. To our knowledge, this is the first report that a bacterium actively enhances the mechanical stability of its cytoplasmic membrane by ubiquinone accumulation to withstand osmotic stress. Should these findings extend beyond *E. coli* to other species and possibly other membrane-related stresses, it might be a promising approach to target stress-induced ubiquinone accumulation for the treatment of infectious and other diseases. For instance, recent studies have found that human patients suffering from nephrotic syndrome displayed reduced Q10 levels[42], and a mutation in a Q10 biosynthetic enzyme in mice caused pathological symptoms similar to Parkinson's disease[43]. Finally, induction of Q8 accumulation by elevated salt levels might be an effective strategy for the biotechnological production of this or related compounds[44].

Acknowledgements

We thank Dr. Nicola Zamboni for advice and assistance with MS/MS analyses, Andreas Kühne for assistance with microscopy, and Karl Kochanowski and Dr. Tobias Fuhrer for helpful discussions. Funding was provided by the MetaNetX project of the Swiss Initiative for Systems Biology (SystemsX.ch; http://metanetx.org) evaluated by the Swiss National Science Foundation, and the Swiss Federal Government through the Federal Office of Education and Science.

Author contributions

D.C.S. performed the experiments and analyzed the data. D.C.S. and U.S. designed the research and wrote the paper.

Figure legends

Figure 1 | Analysis of the salt-induced metabolic changes in *E. coli* by mass spectrometry. (**a**) Maximum exponential growth rates of wild-type *E. coli* BW25113 in glucose mineral medium supplemented with increasing salt concentrations. The half-maximal inhibitory concentration (IC_{50}) was calculated by fitting a Hill-type model to the data (solid line). Data points and error bars represent mean and standard deviation of three biological replicates. Blue circles indicate salt concentrations used in the subsequent metabolomics experiment. (**b**) *E. coli* was cultivated in glucose mineral medium with the indicated salt concentrations until an optical density of 1.0. Intracellular metabolites were extracted from four biological replicates with hot water and measured in technical duplicates by non-targeted flow injection time-of-flight MS[17]. (**c**) Effect of increasing salt concentration in the growth medium on selected intracellular metabolites in exponentially growing *E. coli*. Compounds were annotated as [M-H^+] derivatives with 0.001 Da mass tolerance, and levels were normalized to the 50 mM NaCl values. Data points and error bars represent mean and standard deviation of four biological and two technical replicates (n = 8). [a]Ambiguous sum formula, see **Supplementary Dataset 2** for alternative annotations.

Figure 2 | The global metabolic response of *E. coli* to hyperosmotic stress. (**a**) *K*-means clustering of the log-transformed annotated ion responses normalized to the 50 mM NaCl condition. A number of k = 4 clusters was specified and ions were assigned to the clusters based on squared Euclidean distance. The ions in the strong response cluster 3 were re-clustered based on correlation with k = 2, giving clusters 3a (response already at low NaCl levels) and 3b (response only at higher NaCl levels). The black line represents the centroid of each cluster, and n is the number of ions. (**b**) Metabolic pathway enrichment analysis of clusters 1, 3, 3a, 3b and 4 of the *k*-means clustering shown in (a), sorted by hierarchical clustering based on *p*-values. Pathway definitions from KEGG specific for *E. coli*

were used[45], and the statistical significance of each enriched pathway was calculated with a hypergeometric test with a threshold of $p < 0.0001$. For each pathway, both the *p*-value and the average fold change of the respective metabolites are represented by color intensity.

Figure 3 | The ubiquinone pool and its precursors increase upon osmotic stress. (**a**) Points and error bars represent mean and standard deviation of indicated metabolites in four biological and two technical replicates ($n = 8$). Curves are colored according to the cluster membership of each metabolite in the *k*-means clustering (see **Fig. 2**). Compounds were annotated as electrospray derivatives with 0.001 Da mass tolerance. [a]Ambiguous sum formula, see **Supplementary Dataset 2** for alternative annotations. [b]Additional evidence for annotation by MS/MS fragment ion spectra (**Supplementary Fig. 2**). [c]Compound previously not identified in *E. coli*. (**b**) Response of detected phosphatidyl and prenyl lipids to hyperosmotic stress. Compounds highlighted in bold are intermediates in the ubiquinone-8 biosynthesis pathway. Phospholipids nomenclature: PA, phosphatidic acid; PS, phosphatidylserine; PE, phosphatidylethanolamine; PI, phosphatidylinositol; PME, phosphatidylmethylethanolamine; digits preceding the colon, number of carbon atoms in the acyl side chains; digits following the colon, number of double bonds in the acyl side chains. Octa-PMeOHMoBQ, 2-Octaprenyl-3-methyl-5-hydroxy-6-methoxy-1,4-benzoquinone. *, ** and *** indicate *p*-values (two-sided *t*-test) of < 0.05, < 0.01, < 0.001, respectively. Complete data and *p*-values are presented in **Supplementary Dataset 3**. (**c**) Ratios of indicated lipids in *E. coli* grown with 50 mM NaCl and 450 mM NaCl, inferred from absolute quantification using lipid standards and ^{13}C-labeled internal metabolite standard for matrix effect correction. PE and PG together typically account for ~95% of all *E. coli* membrane lipids[46]. Calibration curves and details to lipid quantification are presented in **Supplementary Fig. 3**.

Figure 4 | Ubiquinone is required for osmotic stress tolerance *in vivo*. (**a**) Open symbols and error bars represent mean and standard deviation of two replicates of each of two independently constructed mutants (n = 4), closed circles the calculated IC_{50} values and lines the best fit of a Hill-type model to the data. Δ*ubiG* + Q10 is the Δ*ubiG* mutant supplemented with 0.2 µM Q10. (**b**) IC_{50} values from panel (a). *tre*$^-$ indicates the mean and standard deviation of the IC_{50}–values of Δ*galU*, Δ*otsA* and Δ*otsB* mutants unable to synthesize trehalose. p indicates statistical significance (left-tail t-test). (**c**) Cell volume V and sphericity S after osmotic shock were determined by microscopy. Δ*ubiG* + Q10 is the Δ*ubiG* mutant supplemented with 20 µM Q10. Data points and error bars represent mean and standard deviation of data from at least 15 cells. Starred values indicate statistical significance (p < 0.05, left-tail t-test). (**d**) Micrographs of *E. coli* cells after osmotic shocks. (**e**) Ubiquinones used in this study. (**f**) Cell volumes of *wt* and the Δ*ubiG* mutant grown in presence of 20 µM of ubiquinones with different polyprenyl chain lengths, determined after an acute osmotic shock with 800 mM NaCl. Open triangles and error bars represent mean and standard deviation of data from at least 15 Δ*ubiG* cells. The horizontal dashed line and shaded area represent mean and standard deviation of wild-type cell volume (n = 23). Starred values indicate significantly smaller cell size than wild-type (p < 0.05, left-tail t-test).

Figure 5 | Ubiquinone enhances the stability of artificial liposomes. (**a**) Light microscopy images of artificial liposomes containing 0% (w/w) Q10 (upper panels) or 5% (w/w) Q10 (lower panels) in the lipid mixture after no osmotic shock (left panels) or a strong osmotic shock with 1000 mM NaCl (right panels). In each panel, fluorescence of the liposome-localized lipid dye FM1-43, bright field images (BF), merged images as well as a 10x zoom into the indicated region of the merged image showing a representative particle are shown. Note that the overall liposome formation efficiency was considerably enhanced by the presence of Q10. (**b**) Method of assessing liposome intactness after osmotic shock. Particles in the microscopy images were detected and classified into liposomes or debris by fitting the shown model images. If the circular shape achieved the best fit particles were

classified as liposomes, whereas if either of the straight lines achieved the best fit particles were classified as debris. The quality of each fit was assessed by root-mean-square deviation (RMSD) between particles and model images. (**c**) Fractions of liposomes with different Q10 contents (percentage values refer to weight-%) resisting acute osmotic shocks with indicated NaCl concentrations. An average of 58 and not less than 15 particles were analyzed per condition. Liposome stability was also enhanced by non-quinone isoprenoids (**Supplementary Fig. 6**).

Online methods

Metabolomics. *E. coli* BW25113 was aerobically cultivated in M9 mineral medium containing 7.52 g $Na_2HPO_4 \cdot 2H_2O$, 3 g KH_2PO_4, 0.5 g NaCl, 2.5 g $(NH_4)_2SO_4$, 14.7 mg $CaCl_2 \cdot 2H_2O$, 246.5 mg $MgSO_4 \cdot 7H_2O$, 16.2 mg $Fe(III)Cl_3 \cdot 6H_2O$, 180 µg $ZnSO_4 \cdot 7H_2O$, 120 µg $CuCl_2 \cdot 2H_2O$, 120 µg $MnSO_4 \cdot H_2O$, 180 µg $CoCl_2 \cdot 6H_2O$ and 1 mg thiamine·HCl per liter of deionized water, supplemented with 4 g/L glucose as carbon source as well as different NaCl concentrations (50, 100, 200, 300, 400, and 500 mM). All these and subsequently mentioned compounds were obtained from Sigma Aldrich (St. Louis, MO, U.S.A.) at the highest available purity (typically ≥95%). Culture volume was 1 mL in deep 96-well plates, temperature was 37° C and agitation was 300 rpm on an orbital shaker. Four independent cultures per NaCl concentrations were grown until reaching an optical density at 600 nm of 1.0 Cells were then harvested by centrifugation (5 min, 0° C, 4,500 rcf) and intracellular metabolites were extracted by adding 150 µL of deionized water heated to 80° C for 10 min. Debris were removed by centrifugation, and samples were analyzed by flow-injection time-of-flight MS with an Agilent 6550 QToF instrument (Agilent, Santa Clara, CA, U.S.A.) operated in negative ionization mode at 4 GHz high-resolution in a range from 50-1,000 *m/z* using published settings[17]. The mobile phase was 60:40 isopropanol:water (v/v) and 1 mM NH_4F at pH 9.0 supplemented with 10 nM hexakis(1H, 1H, 3H- tetrafluoropropoxy)phosphazine and 80 nM taurocholic acid for online mass correction. Spectral processing and ion annotation based on accurate mass within 0.001 Da using the KEGG eco database[45] as reference and accounting for $[M\text{-}H^+]$, $[M+F^-]$, [.H/Na M-H^+] and [H/Na M+F^-] ions were performed using Matlab R2012b (The Mathworks, Nattick, MA, U.S.A.) as described previously[17].

Lipidomics. Lipids were extracted from exponentially growing *E. coli* BW25113 cells at OD_{600} = 1.0 using a two-step extraction procedure with 17:1 $CHCL_3$:methanol (v/v) for non-polar and 2:1 $CHCL_3$:methanol (v/v) for polar lipids as described previously[22]. Extracted lipids from 413 mg dry cell weight were vacuum-dried, resuspended in 1:1 acetonitrile:methanol, spiked with fully ^{13}C-labeled *E.*

coli extract for matrix effect correction and analyzed by flow-injection MS as described previously[17]. Absolute concentrations were inferred from $^{12}C/^{13}C$ ratios of respective lipids using a calibration curve of lipid standards processed in the same way (**Supplementary Fig. 3**).

Compound identification by MS/MS. MS/MS spectra were acquired on an Agilent 6550 QTOF mass spectrometer operated in negative ionization mode, with instrument settings as described previously[17]. Precursor ions of selected compounds were targeted as $[M\text{-}H^+]$ electrospray derivatives with a window size of $\pm$ 2 *m/z* in Q_1. Fragmentation of the precursor ion was performed by collision-induced dissociation at 40 eV collision energy. Fragment ion spectra were recorded in scanning mode by high-resolution TOF MS. Peaks with intensity of at least 10% of the highest non-saturated peak intensity in the MS/MS spectra were extracted and matched with compounds in the PubChem database using MetFrag[47]. A top rank of the target compound among all matching compounds in the database was considered as further evidence for the initially proposed annotation based on accurate mass.

Unsupervised data analysis. All steps of data analysis were performed using Matlab R2012b. *K*-means clustering was performed on all 535 annotated ions over salt concentration using the squared Euclidean distance metric. A number of $k = 4$ clusters was specified to capture broad classes of salt-dependent changing ions. Metabolic pathway enrichment analysis was based on KEGG pathway definitions[45] using only pathways occurring in *E. coli*. For each pathway, we first counted how many metabolites were present in the respective *k*-means cluster and secondly computed the hypergeometric probability of the enrichment (*hygepdf* function in Matlab) as described previously[48]. All non-significantly enriched pathways with $P \geq 0.0001$ were not considered.

Growth physiology experiments. *E. coli* BW25113 and its respective deletion mutants were obtained from the KEIO collection[49], and always both independent clones were analyzed to rule out genetic errors. Growth medium always was glucose M9 mineral medium supplemented with different concentrations of NaCl or ubiquinone-10 (Sigma Aldrich, C9538, ≥98% purity) where

indicated. Growth was monitored by cultivating cells in 200 µL medium shaking at 37° C in a TECAN Infinite M200 plate reading instrument (TECAN Group, Männedorf, Switzerland) and measuring the absorbance at 600 nm every 10 min over a period of at least 24 h.

ROS assay. Intracellular ROS levels were measured using the dihydroethidium (DHE) assay as described previously[50]. Briefly, preculture cells were grown in glucose M9 mineral medium with the indicated salt concentrations until reaching an optical density of 1.0 in mid-exponential phase. 100 µL of this culture were transferred to a 96-well plate and mixed with 100 µL of pre-warmed fresh medium containing 20 µM of DHE (Sigma Aldrich, product code D7008, ≥95% purity). Cells were subsequently incubated at 37° C for 5 h to allow uptake and eventual oxidation of DHE by ROS. DHE oxidation was measured by fluorescence (excitation wavelength: 485 nm; emission wavelength: 595 nm) using a TECAN Infinite M200 plate reading device. Background fluorescence from sterile medium containing 10 µM DHE was subtracted from the sample values.

Morphotyping experiments. Cells were grown at 37° C in M9 glucose medium supplemented with 20 µM 2,3-Dimethoxy-5-methyl-*p*-benzoquinone (Q0, Sigma Aldrich, D9150, ≥95% purity), ubiquinone-2 (Q2, C8081, ≥90%), ubiquinone-4 (Q4, C2470, ≥90%), ubiquinone-10 (Q10, C9538, ≥98%), geraniol (163333, ≥98%), farnesol (F203, ≥95%), solanesol (S8754, ≥90%) or lycopene (L9879, ≥90%) when indicated until mid-exponential growth phase (OD_{600} = 1.0 ± 0.2). 5 µL of cell suspension were transferred to borosilicate microscopy slides, and 5 µL of buffer (10 mM TrisHCl pH 7.4 supplemented with different NaCl concentrations) were added to reach indicated osmotic shock strengths. Cell imaging by microscopy and image analysis were performed as described below.

Preparation of artificial liposomes. Liposomes were prepared from a lipid mixture containing 45% phosphatidylcholine (Sigma Aldrich, P3556, ≥99% purity), 25% phosphatidylethanolamine (P8068, ≥98%), 20% phosphatidylinositol (P6636, ≥50%) and 10% phosphatidic acid (P9511, ≥98%), with ubiquinone-10 (C9538, ≥98%), solanesol (S8754, ≥90%) or lycopene (L9879, ≥90%) replacing the other lipids as indicated. The lipid mixture contained 0.02% of the fluorescent lipid dye FM1-43

(SynaptoGreen, Sigma Aldrich, S6814, ≥95%). All percentage values refer to weight-%. Overall, the lipid composition thus was representative for a biological lipid bilayer membrane. Liposomes were prepared using a solvent evaporation - rehydration approach published previously[51]. The liposome formation buffer contained 5 mM Tris Base, 30 mM K_3PO_4, 30 mM KH_2PO_4, 1 mM $MgSO_4$, 0.5 mM EDTA, 1% glycerol, and pH was adjusted to 7.8 with KOH. Liposomes of 1 mg/mL total lipids were allowed to form for 5 min on borosilicate microscope slides, and subsequently formation buffer supplemented with NaCl was added to reach the indicated external salt concentrations.

Fluorescence microscopy and image analysis. Microscopy of artificial liposomes and living *E. coli* cells was performed within 5 min after NaCl addition using a Nikon Eclipse Ti inverted epifluorescence microscope equipped with a CoolLED PrecisExcite light source and a Nikon 60x oil immersion objective providing a total magnification of 600-fold. Filters used for fluorescence imaging of FM1-43 were 470 ± 40 nm (excitation) and 525 ± 50 nm (emission), respectively, and exposure time was set to 2.5 s. Image acquisition and basic analysis (brightness and contrast optimization, image sharpening) were performed using µManager[52] and ImageJ[53], respectively. For the liposome experiment, detection and classification of particles larger than 100 pixels was performed using Matlab. To each detected particle five prototypic image patterns were fitted (shown in **Fig. 5**), and the root-mean-square deviation (RMSD) of each fit was computed. The image with lowest RMSD was used to classify the particle into liposome (in case the circular shape fit had lowest RMSD) or debris (in case one of the four straight lines had lowest RMSD). Particles with RMSD > 0.3 (usually several liposomes in very close proximity or U-shaped debris leading to false classification) were re-classified by visual inspection. At least 15 and on average 58 particles were classified for each experimental condition. For cell volume determination, bright-field images of cells were acquired using a Nikon 100x oil immersion objective providing a total magnification of 1,000-fold. The geometry and volume of individual cells was calculated by assuming cylindrical shape and measuring cell length and diameter based on a 10 µm micro-ruler. At least 15 cells per condition were analyzed.

Statistical analysis. Statistical analysis of data was performed using Matlab R2012b and functions embedded in the Bioinformatics and Statistics toolboxes. The types of statistical tests used and the returned *P*-values are indicated when referring to these tests.

References

1. Bartlett, D. H. Pressure effects on in vivo microbial processes. *Biochim. Biophys. Acta* **1595,** 367–381 (2002).

2. Record Jr., M. T., Courtenay, E. S., Cayley, D. S. & Guttman, H. J. Responses of E. coli to osmotic stress: large changes in amounts of cytoplasmic solutes and water. *Trends Biochem. Sci.* **23,** 143–8 (1998).

3. Vreeland, R. H. Mechanisms of halotolerance in microorganisms. *Crit. Rev. Microbiol.* **14,** 311–56 (1987).

4. Krämer, R. Bacterial stimulus perception and signal transduction: response to osmotic stress. *Chem. Rec.* **10,** 217–29 (2010).

5. Piuri, M., Sanchez-Rivas, C. & Ruzal, S. M. Cell wall modifications during osmotic stress in Lactobacillus casei. *J. Appl. Microbiol.* **98,** 84–95 (2005).

6. Wood, J. M. Bacterial osmoregulation: a paradigm for the study of cellular homeostasis. *Annu. Rev. Microbiol.* **65,** 215–38 (2011).

7. Calamita, G., Bishai, W. R., Preston, G. M., Guggino, W. B. & Agre, P. Molecular cloning and characterization of AqpZ, a water channel from Escherichia coli. *J. Biol. Chem.* **270,** 29063–6 (1995).

8. Laimins, L. A., Rhoads, D. B. & Epstein, W. Osmotic control of kdp operon expression in Escherichia coli. *Proc. Natl. Acad. Sci.* **78,** 464–468 (1981).

9. Grothe, S., Krogsrud, R. L., McClellan, D. J., Milner, J. L. & Wood, J. M. Proline transport and osmotic stress response in Escherichia coli K-12. *J. Bacteriol.* **166,** 253–9 (1986).

10. Von Weymarn, N., Nyyssölä, a., Reinikainen, T., Leisola, M. & Ojamo, H. Improved osmotolerance of recombinant Escherichia coli by de novo glycine betaine biosynthesis. *Appl. Microbiol. Biotechnol.* **55,** 214–218 (2001).

11. Giaever, H. M., Styrvold, O. B., Kaasen, I. & Strom, A. R. Biochemical and genetic characterization of Osmoregulatory Trehalose Synthesis in Escherichia coli. *J. Bacteriol.* **170,** 2841–2849 (1988).

12. Elbein, A. D., Pan, Y. T., Pastuszak, I. & Carroll, D. New insights on trehalose: a multifunctional molecule. *Glycobiology* **13,** 17R–27R (2003).

13. Klein, W., Ehmann, U. & Boos, W. The repression of trehalose transport and metabolism in Escherichia coli by high osmolarity is mediated by trehalose-6-phosphate phosphatase. *Res. Microbiol.* **142,** 359–71 (1991).

14. Cayley, S. & Record, M. T. Large changes in cytoplasmic biopolymer concentration with osmolality indicate that macromolecular crowding may regulate protein-DNA interactions and growth rate in osmotically stressed Escherichia coli K-12. *J. Mol. Recognit.* **17,** 488–96 (2004).

15. Horta, B. a C., Perić-Hassler, L. & Hünenberger, P. H. Interaction of the disaccharides trehalose and gentiobiose with lipid bilayers: a comparative molecular dynamics study. *J. Mol. Graph. Model.* **29,** 331–46 (2010).

16. Pereira, C. S. & Hünenberger, P. H. Effect of trehalose on a phospholipid membrane under mechanical stress. *Biophys. J.* **95,** 3525–34 (2008).

17. Fuhrer, T., Heer, D., Begemann, B. & Zamboni, N. High-Throughput, Accurate Mass Metabolome Profiling of Cellular Extracts by Flow Injection-Time-of-Flight Mass Spectrometry. *Anal. Chem.* **83,** 7074–80 (2011).

18. Landis, L., Xu, J. & Johnson, R. C. The cAMP receptor protein CRP can function as an osmoregulator of transcription in Escherichia coli. *Genes Dev.* **13,** 3081–3091 (1999).

19. Balsalobre, C., Johansson, J. & Uhlin, B. E. Cyclic AMP-dependent osmoregulation of crp gene expression in Escherichia coli. *J. Bacteriol.* **188,** 5935–44 (2006).

20. Shen, B., Hohmann, S., Jensen, R. G. & Bohnert, H. J. Roles of sugar alcohols in osmotic stress adaptation. Replacement of glycerol by mannitol and sorbitol in yeast. *Plant Physiol.* **121,** 45–52 (1999).

21. Gunasekera, T. S., Csonka, L. N. & Paliy, O. Genome-wide transcriptional responses of Escherichia coli K-12 to continuous osmotic and heat stresses. *J. Bacteriol.* **190,** 3712–20 (2008).

22. Ejsing, C. S. *et al.* Global analysis of the yeast lipidome by quantitative shotgun mass spectrometry. *Proc. Natl. Acad. Sci. U. S. A.* **106,** 2136–41 (2009).

23. Søballe, B. & Poole, R. K. Ubiquinone limits oxidative stress in Escherichia coli. *Microbiology* **146,** 787–96 (2000).

24. Smirnova, G. V, Muzyka, N. G. & Oktyabrsky, O. N. The role of antioxidant enzymes in response of Escherichia coli to osmotic upshift. *FEMS Microbiol. Lett.* **186,** 209–13 (2000).

25. Kalir, A. & Poljakoff-Mayber, A. Changes in Activity of Malate Dehydrogenase, Catalase , Peroxidase and Superoxide Dismutase in Leaves of Halimione portulacoides (L.) Aellen Exposed to High Sodium Chloride Concentrations. *Ann. Bot.* **47,** 75–85 (1981).

26. Stroobant, P., Young, I. G. & Gibson, F. Mutants of Escherichia coli K-12 Blocked in the Final Reaction of Ubiquinone Biosynthesis: Characterization and Genetic Analysis. *J. Bacteriol.* **109,** 134–139 (1972).

27. Kanai, T., Takahashi, K. & Inoue, H. Three distinct-type glutathione S-transferases from Escherichia coli important for defense against oxidative stress. *J. Biochem.* **140,** 703–11 (2006).

28. Wu, G., Williams, H. D., Gibson, F. & Poole, K. Mutants of Escherichia coli affected in respiration: the cloning and nucleotide sequence of ubiA, encoding the membrane-bound p-hydroxybenzoate:octaprenyltransferase. *J. Gen. Microbiol.* **139,** 1795–1805 (1993).

29. Pilizota, T. & Shaevitz, J. W. Fast, multiphase volume adaptation to hyperosmotic shock by Escherichia coli. *PLoS One* **7,** e35205 (2012).

30. Paturej, J., Popova, H., Milchev, A. & Vilgis, T. A. Force-induced breakdown of flexible polymerized membrane. *arXiv:1111.6719v3* (2012).

31. Katsikas, H. & Quinn, P. J. The Polyisoprenoid Chain Length Influences the Interaction of Ubiquinones with Phospholipid Bilayers. *Biochim. Biophys. Acta* **689,** 363–369 (1982).

32. Roche, Y., Peretti, P. & Bernard, S. Influence of the chain length of ubiquinones on their interaction with DPPC in mixed monolayers. *Biochim. Biophys. Acta* **1758,** 468–78 (2006).

33. De Rosa, M., Gambacorta, A. & Gliozzi, A. Structure, biosynthesis, and physicochemical properties of archaebacterial lipids. *Microbiol. Rev.* **50,** 70–80 (1986).

34. Konings, W. N., Albers, S.-V., Koning, S. & Driessen, A. J. M. The cell membrane plays a crucial role in survival of bacteria and archaea in extreme environments. *Antonie Van Leeuwenhoek* **81,** 61–72 (2002).

35. Jacquemet, A., Barbeau, J., Lemiègre, L. & Benvegnu, T. Archaeal tetraether bipolar lipids: Structures, functions and applications. *Biochimie* **91,** 711–717 (2009).

36. Houssin, C., Eynard, N., Shechter, E. & Ghazi, A. Effect of osmotic pressure on membrane energy-linked functions in Escherichia coli. *Biochim. Biophys. Acta* **1056,** 76–84 (1991).

37. Jensen, M. Ø. & Mouritsen, O. G. Lipids do influence protein function-the hydrophobic matching hypothesis revisited. *Biochim. Biophys. Acta* **1666,** 205–26 (2004).

38. Stachowiak, J. C. *et al.* Membrane bending by protein-protein crowding. *Nat. Cell Biol.* **14,** 944–9 (2012).

39. Haines, T. H. Do sterols reduce proton and sodium leaks through lipid bilayers? *Prog. Lipid Res.* **40,** 299–324 (2001).

40. Gruszecki, W. I., Smal, A. & Szymczuk, D. The effect of zeaxanthin on the thickness of dimyristoylphosphatidylcholine bilayer: X-ray diffraction study. *J. Biol. Phys.* **18,** 271–280 (1992).

41. Ma, Y. *et al.* Study of the effect of membrane thickness on microcapsule strength, permeability, and cell proliferation. *J. Biomed. Mater. Res. A* **101,** 1007–15 (2013).

42. Gasser, D. L. *et al.* Focal segmental glomerulosclerosis is associated with a PDSS2 haplotype and, independently, with a decreased content of coenzyme Q10. *Am. J. Physiol. Renal Physiol.* **305,** F1228–38 (2013).

43. Ziegler, C. G. K. *et al.* Parkinson's disease-like neuromuscular defects occur in prenyl diphosphate synthase subunit 2 (Pdss2) mutant mice. *Mitochondrion* **12,** 248–57 (2012).

44. Yoshida, H., Kotani, Y., Ochiai, K. & Araki, K. Production of ubiquinone-10 using bacteria. *J. Gen. Appl. Microbiol.* **44,** 19–26 (1998).

45. Ogata, H. *et al.* KEGG: Kyoto Encyclopedia of Genes and Genomes. *Nucleic Acids Res.* **27,** 29–34 (1999).

46. Raetz, C. R. Enzymology, Genetics, and Regulation of Membrane Phospholipid Synthesis in Escherichia coli. *Microbiol. Mol. Biol. Rev.* **42,** 614–659 (1978).

47. Wolf, S., Schmidt, S., Müller-Hannemann, M. & Neumann, S. In silico fragmentation for computer assisted identification of metabolite mass spectra. *BMC Bioinformatics* **11,** 148 (2010).

48. Kankainen, M., Gopalacharyulu, P., Holm, L. & Oresic, M. MPEA--metabolite pathway enrichment analysis. *Bioinformatics* **27,** 1878–9 (2011).

49. Baba, T. *et al.* Construction of Escherichia coli K-12 in-frame, single-gene knockout mutants: the Keio collection. *Mol. Syst. Biol.* **2,** 2006.0008 (2006).

50. Klinger, H. *et al.* Quantitation of (a)symmetric inheritance of functional and of oxidatively damaged mitochondrial aconitase in the cell division of old yeast mother cells. *Exp. Gerontol.* **45,** 533–42 (2010).

51. Karlsson, M. *et al.* Electroinjection of colloid particles and biopolymers into single unilamellar liposomes and cells for bioanalytical applications. *Anal. Chem.* **72,** 5857–62 (2000).

52. Edelstein, A., Amodaj, N., Hoover, K., Vale, R. & Stuurman, N. Computer control of microscopes using μManager. *Curr. Protoc. Mol. Biol.* **92,** 14.20.1 – 14.20.17 (2010).

53. Schneider, C. a, Rasband, W. S. & Eliceiri, K. W. NIH Image to ImageJ: 25 years of image analysis. *Nat. Methods* **9,** 671–675 (2012).

Competing financial interests

The authors declare no competing financial interests.

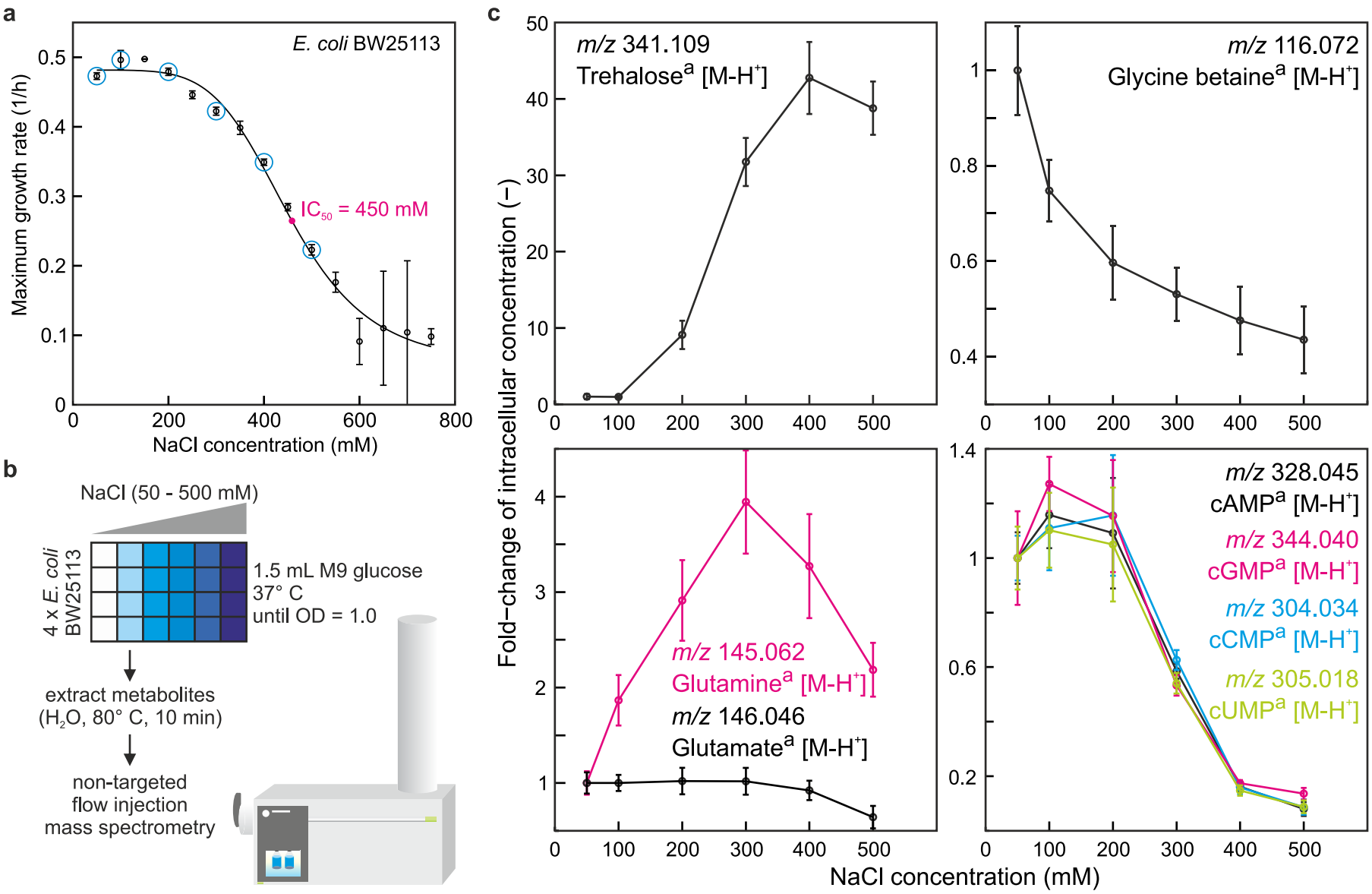
a
E. coli BW25113
Maximum growth rate (1/h)
IC50 = 450 mM
NaCl concentration (mM)
b
NaCl (50 - 500 mM)
4 x E. coli BW25113
1.5 mL M9 glucose
37° C
until OD = 1.0
extract metabolites
(H2O, 80° C, 10 min)
non-targeted
flow injection
mass spectrometry
c
m/z 341.109
Trehalose[a] [M-H+]
m/z 116.072
Glycine betaine[a] [M-H+]
Fold−change of intracellular concentration (−)
m/z 145.062
Glutamine[a] [M-H+]
m/z 146.046
Glutamate[a] [M-H+]
m/z 328.045
cAMP[a] [M-H+]
m/z 344.040
cGMP[a] [M-H+]
m/z 304.034
cCMP[a] [M-H+]
m/z 305.018
cUMP[a] [M-H+]
NaCl concentration (mM)

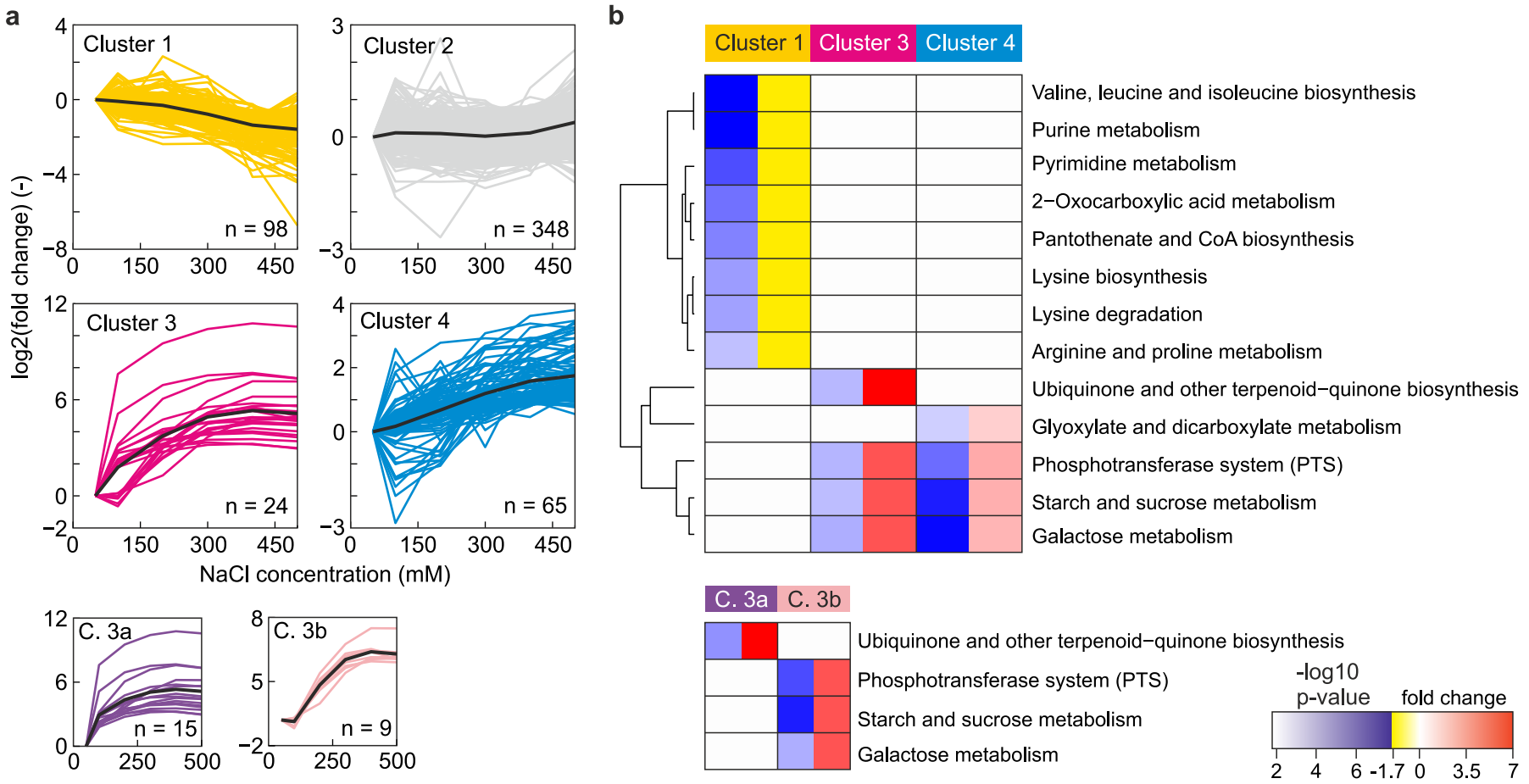
a
Cluster 1
n = 98
Cluster 2
n = 348
Cluster 3
n = 24
Cluster 4
n = 65
log2(fold change) (-)
NaCl concentration (mM)
C. 3a
n = 15
C. 3b
n = 9
b
Cluster 1
Cluster 3
Cluster 4
Valine, leucine and isoleucine biosynthesis
Purine metabolism
Pyrimidine metabolism
2−Oxocarboxylic acid metabolism
Pantothenate and CoA biosynthesis
Lysine biosynthesis
Lysine degradation
Arginine and proline metabolism
Ubiquinone and other terpenoid−quinone biosynthesis
Glyoxylate and dicarboxylate metabolism
Phosphotransferase system (PTS)
Starch and sucrose metabolism
Galactose metabolism
C. 3a
C. 3b
Ubiquinone and other terpenoid−quinone biosynthesis
Phosphotransferase system (PTS)
Starch and sucrose metabolism
Galactose metabolism
-log10
p-value
fold change

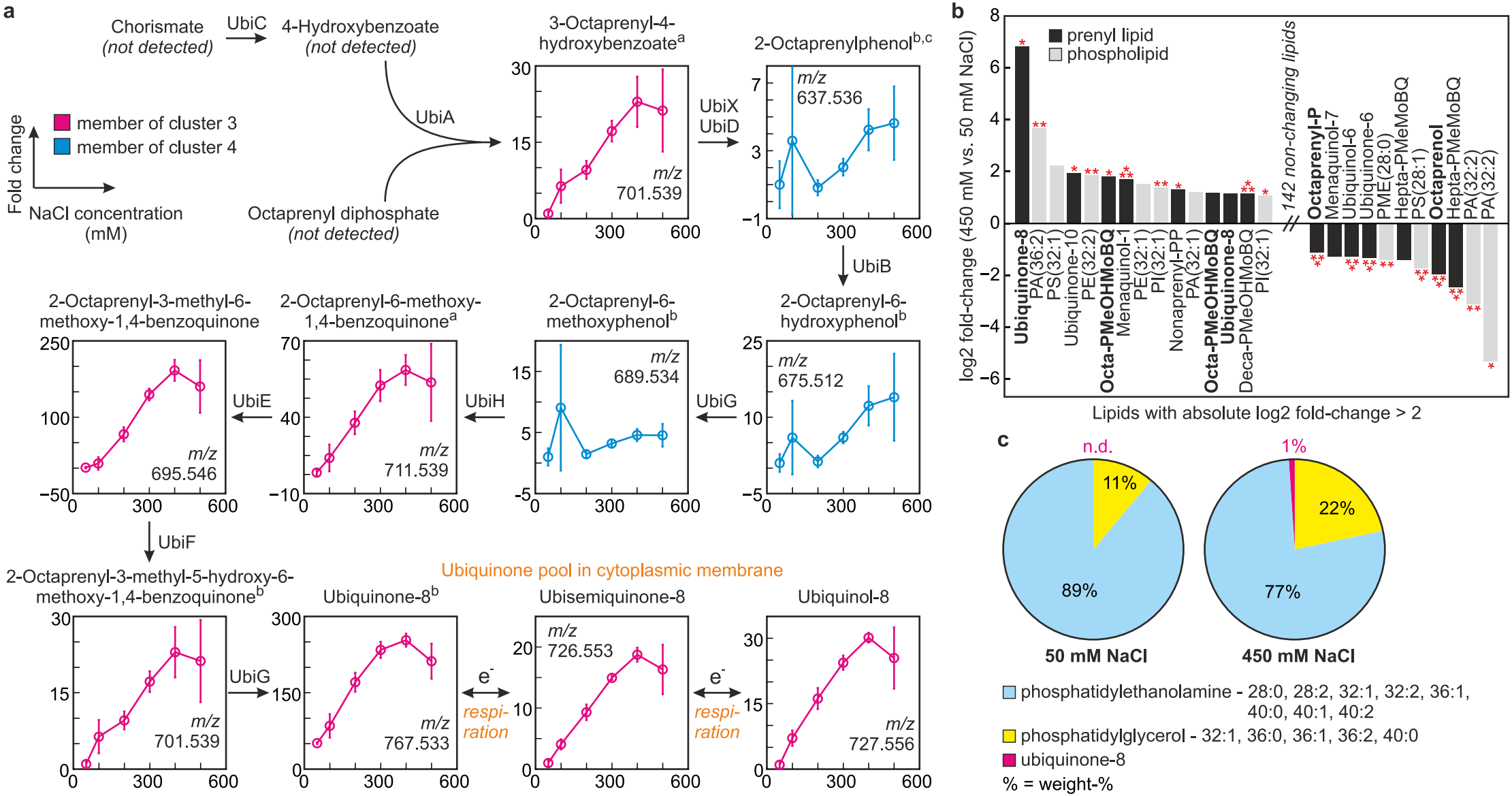
a
Chorismate
(not detected)
UbiC
4-Hydroxybenzoate
(not detected)
UbiA
Octaprenyl diphosphate
(not detected)
member of cluster 3
member of cluster 4
Fold change
NaCl concentration
(mM)
3-Octaprenyl-4-hydroxybenzoate[a]
m/z 701.539
UbiX
UbiD
2-Octaprenylphenol[b,c]
m/z 637.536
UbiB
2-Octaprenyl-6-hydroxyphenol[b]
m/z 675.512
UbiG
2-Octaprenyl-6-methoxyphenol[b]
m/z 689.534
UbiH
2-Octaprenyl-6-methoxy-1,4-benzoquinone[a]
m/z 711.539
UbiE
2-Octaprenyl-3-methyl-6-methoxy-1,4-benzoquinone
m/z 695.546
UbiF
2-Octaprenyl-3-methyl-5-hydroxy-6-methoxy-1,4-benzoquinone[b]
m/z 701.539
UbiG
Ubiquinone pool in cytoplasmic membrane
Ubiquinone-8[b]
m/z 767.533
e-
respi-ration
Ubisemiquinone-8
m/z 726.553
e-
respi-ration
Ubiquinol-8
m/z 727.556
b
log2 fold-change (450 mM vs. 50 mM NaCl)
prenyl lipid
phospholipid
142 non-changing lipids
Ubiquinone-8
PA(36:2)
PS(32:1)
Ubiquinone-10
PE(32:2)
Octa-PMeOHMoBQ
Menaquinol-1
PE(32:1)
PI(32:1)
Nonaprenyl-PP
PA(32:1)
Octa-PMeOHMoBQ
Ubiquinone-8
Deca-PMeOHMoBQ
PI(32:1)
Octaprenyl-P
Menaquinol-7
Ubiquinol-6
Ubiquinone-6
PME(28:0)
Hepta-PMeMoBQ
PS(28:1)
Octaprenol
Hepta-PMeMoBQ
PA(32:2)
PA(32:2)
Lipids with absolute log2 fold-change > 2
c
n.d.
11%
89%
50 mM NaCl
1%
22%
77%
450 mM NaCl
phosphatidylethanolamine - 28:0, 28:2, 32:1, 32:2, 36:1, 40:0, 40:1, 40:2
phosphatidylglycerol - 32:1, 36:0, 36:1, 36:2, 40:0
ubiquinone-8
% = weight-%

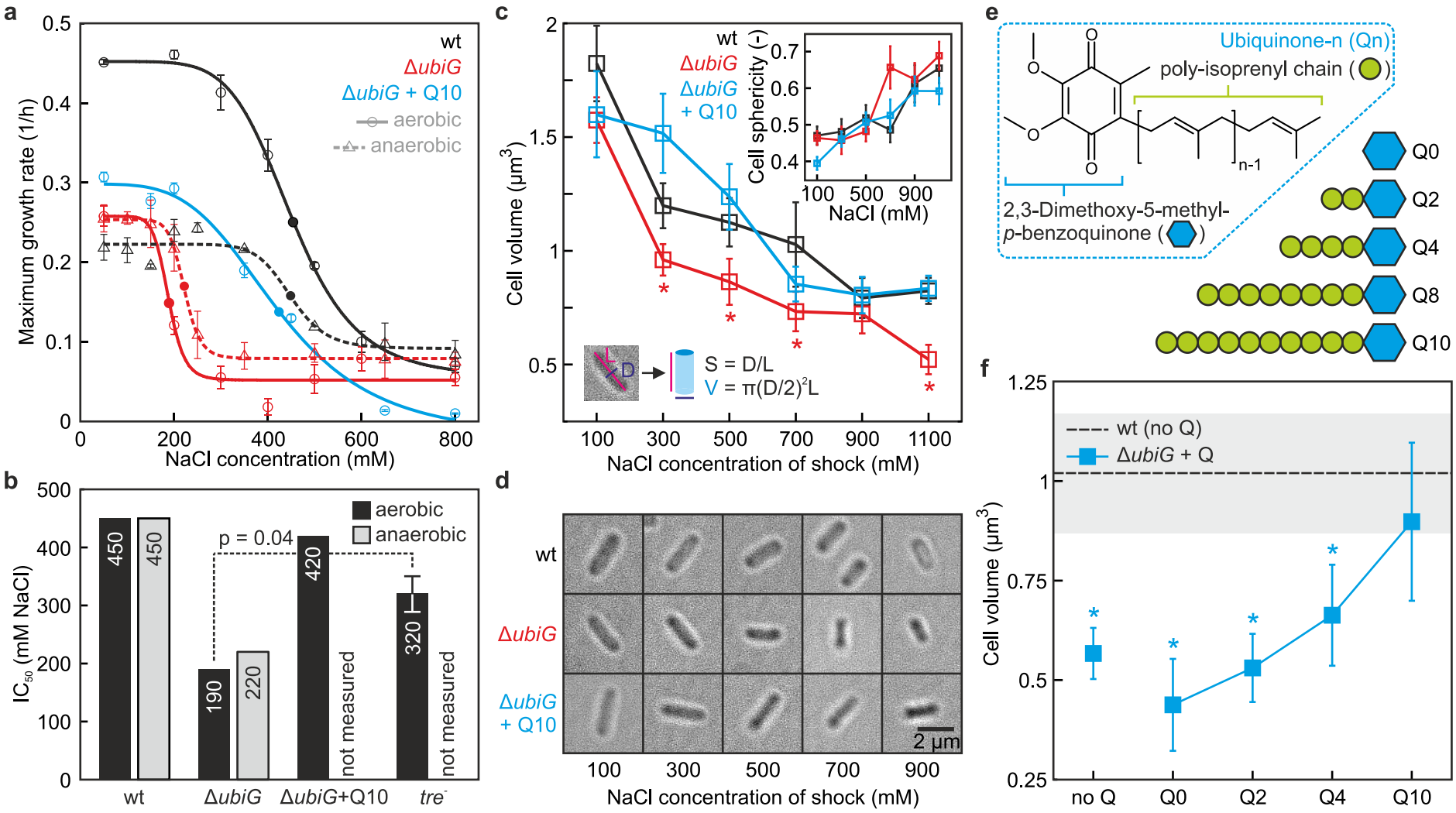
a
Maximum growth rate (1/h)
NaCl concentration (mM)
wt
ΔubiG
ΔubiG + Q10
aerobic
anaerobic
b
IC50 (mM NaCl)
aerobic
anaerobic
p = 0.04
450
450
190
220
420
not measured
320
not measured
wt
ΔubiG
ΔubiG+Q10
tre-
c
Cell volume (μm3)
Cell sphericity (-)
NaCl (mM)
NaCl concentration of shock (mM)
S = D/L
V = π(D/2)2L
d
wt
ΔubiG
ΔubiG + Q10
2 μm
NaCl concentration of shock (mM)
e
Ubiquinone-n (Qn)
poly-isoprenyl chain
2,3-Dimethoxy-5-methyl-p-benzoquinone
Q0
Q2
Q4
Q8
Q10
f
Cell volume (μm3)
wt (no Q)
ΔubiG + Q
no Q
Q0
Q2
Q4
Q10

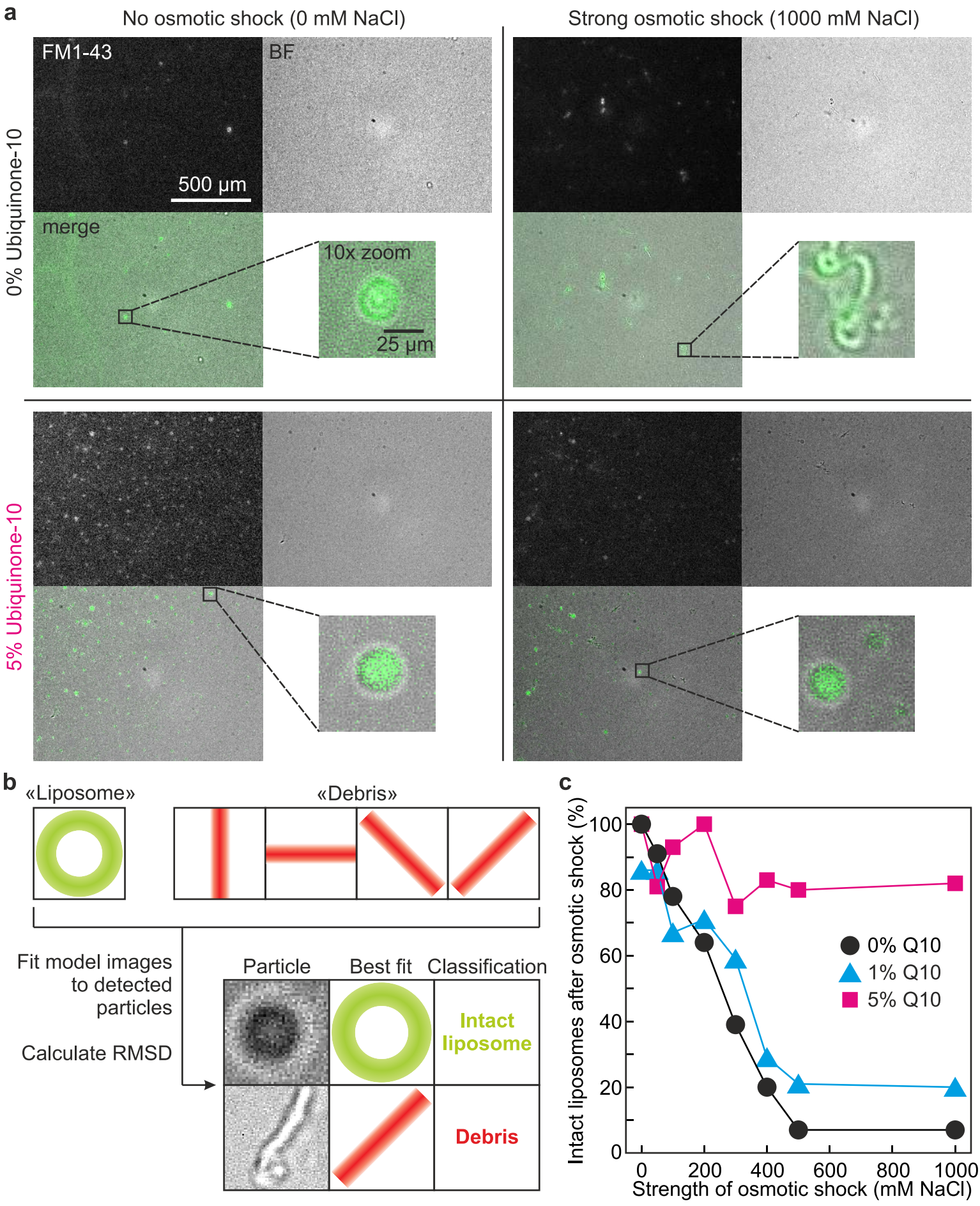
a
No osmotic shock (0 mM NaCl)
Strong osmotic shock (1000 mM NaCl)
0% Ubiquinone-10
5% Ubiquinone-10
FM1-43
BF
500 µm
merge
10x zoom
25 µm
b
«Liposome»
«Debris»
Fit model images to detected particles
Calculate RMSD
Particle
Best fit
Classification
Intact liposome
Debris
c
Intact liposomes after osmotic shock (%)
Strength of osmotic shock (mM NaCl)
0% Q10
1% Q10
5% Q10
0
20
40
60
80
100
0
200
400
600
800
1000

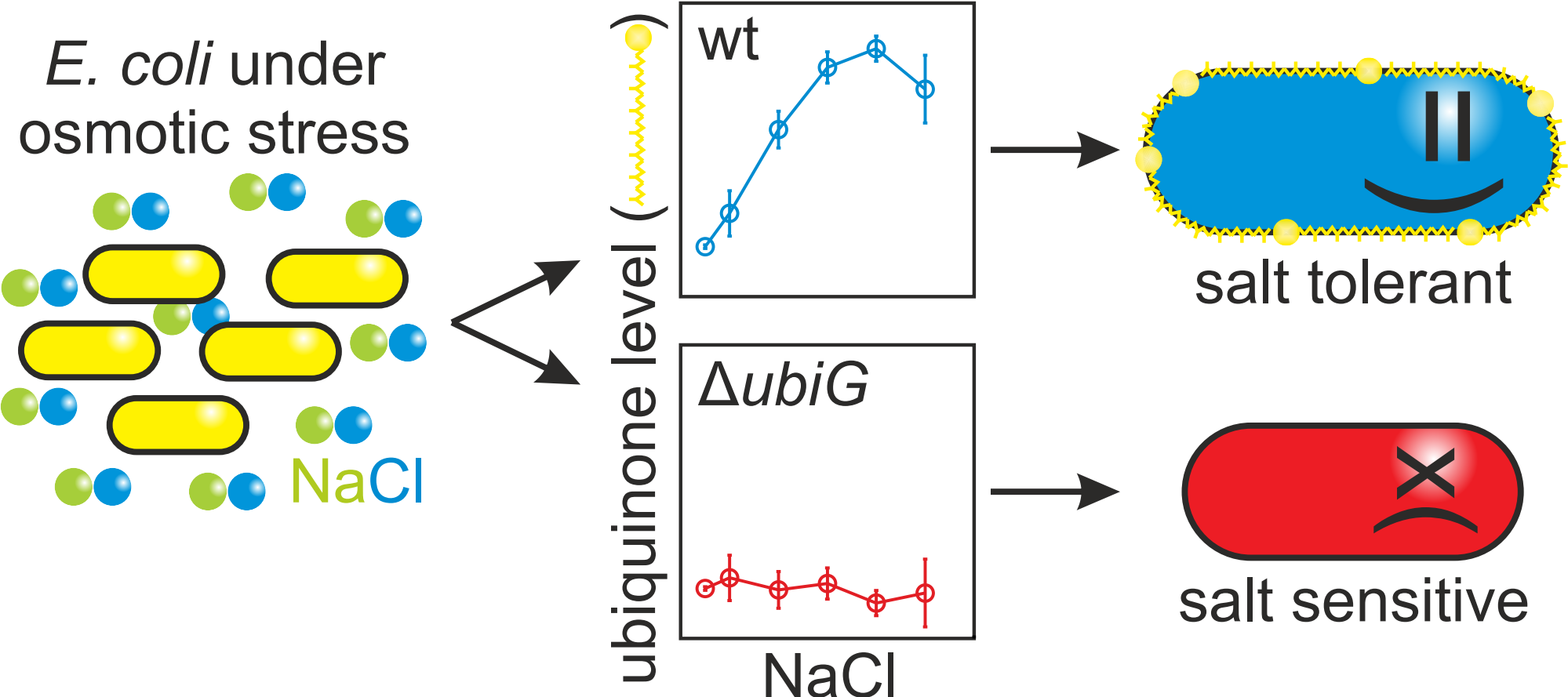
E. coli under osmotic stress
NaCl
ubiquinone level (
wt
ΔubiG
NaCl
salt tolerant
salt sensitive